Diffusion by a Random Velocity Field

Robert H. Kraichnan

Citation: Phys. Fluids **13**, 22 (1970); doi: 10.1063/1.1692799
View online: http://dx.doi.org/10.1063/1.1692799
View Table of Contents: http://pof.aip.org/resource/1/PFLDAS/v13/i1
Published by the American Institute of Physics.

Diffusion by a Random Velocity Field

ROBERT H. KRAICHNAN
Dublin, New Hampshire
(Received 5 June 1969)

Single-particle diffusion in a multivariate-normal, incompressible, stationary, isotropic velocity field is calculated in two and three dimensions by computer simulation and by the direct-interaction approximation. The computer simulations are carried out by storing the velocity field as a set of Fourier components and synthesizing in physical space only along the particle trajectories. The spectra taken for the velocity field are of the form $E(k) \propto \delta(k - k_0)$ and $E(k) \propto k^4 \exp(-2k^2/k_0^2)$ in three dimensions, and $E(k) \propto \delta(k - k_0)$ and $E(k) \propto k^3 \exp(-3k^2/2k_0^2)$ in two dimensions. Both frozen Eulerian fields and fields with Gaussian time correlation are treated. The simulation results agree with Taylor's picture of a classical diffusion process for times long compared with the eddy circulation time, except for the frozen-Eulerian-field runs in two dimensions, where strong trapping effects are found. The direct-interaction approximations for Lagrangian velocity correlation, eddy diffusivity, dispersion, and modal response functions agree well with the computer experiments except where there are trapping effects, which the approximation completely fails to represent.

I. INTRODUCTION

In this paper, we shall compare computer simulation and statistical theory for the diffusion of fluid particles by a divergenceless, statistically stationary, homogeneous, isotropic, multivariate-normal velocity field $\mathbf{u}(\mathbf{x}, t)$ in both two and three dimensions. A particle started at $\mathbf{x} = 0$, $t = 0$ follows the trajectory $\mathbf{y}(t)$ determined by

$$\frac{d\mathbf{y}(t)}{dt} = \mathbf{v}(t), \qquad \mathbf{v}(t) = \mathbf{u}(\mathbf{y}, t), \qquad \mathbf{y}(0) = 0. \tag{1}$$

If this motion is averaged over a statistical ensemble of velocity fields, the probability density that the particle reaches $\mathbf{x}$ at time t is

$$G(\mathbf{x}, t) = \langle \delta^3[\mathbf{x} - \mathbf{y}(t)] \rangle, \tag{2}$$

where $\langle\ \rangle$ denotes ensemble average. $G(\mathbf{x}, t)$ is the Green's function for the evolution of an arbitrary initial probability distribution of particles:

$$\phi(\mathbf{x}, t) = \int G(\mathbf{x} - \mathbf{x}', t)\phi(\mathbf{x}', 0)\, d\mathbf{x}', \tag{3}$$

where $\phi(\mathbf{x}, t)$ is the probability density at time t. The function

$$g_k(t) = \int G(\mathbf{x}, t) \exp(-i\mathbf{k}\cdot\mathbf{x})\, d\mathbf{x}$$

satisfies $g_k(0) = 1$ and describes the evolution of the Fourier components of the initial distribution. The isotropy condition yields

$$g_k(t) = 4\pi k^{-2} \int_0^\infty G(\mathbf{x}, t)(kx) \sin(kx)\, dx \quad \text{(3-D)}, \tag{4}$$

$$g_k(t) = 2\pi k^{-1} \int_0^\infty G(\mathbf{x}, t)(kx) J_0(kx)\, dx \quad \text{(2-D)}, \tag{5}$$

in three and two dimensions [(3-D), (2-D)], respectively. We shall also deal with the Laplace transform

$$G_k(p) = \int_0^\infty \exp(-pt) g_k(t)\, dt. \tag{6}$$

$G_k(0)$ is the relaxation time for an initial distribution $\cos(\mathbf{k}\cdot\mathbf{x})$.

The incompressible, isotropic, multivariate-normal velocity field is fully specified by the covariance scalar $\langle \mathbf{u}(\mathbf{x}, t)\cdot\mathbf{u}(\mathbf{x}', t') \rangle$. We shall consider covariances of the form

$$\langle \mathbf{u}(\mathbf{x} + \mathbf{r}, t)\cdot\mathbf{u}(\mathbf{x}, t') \rangle = 2D(t - t') \int_0^\infty E(k) \frac{\sin(kr)}{kr}\, dk \quad \text{(3-D)}, \tag{7}$$

$$\langle \mathbf{u}(\mathbf{x} + \mathbf{r}, t)\cdot\mathbf{u}(\mathbf{x}, t') \rangle = 2D(t - t') \int_0^\infty E(k) J_0(kr)\, dk \quad \text{(2-D)}, \tag{8}$$

where $E(k)$ is the usual energy spectrum function normalized by

$$\int_0^\infty E(k)\, dk = \frac{3v_0^2}{2} \quad \text{(3-D)}, \quad = v_0^2 \quad \text{(2-D)},$$

where v_0 is the root-mean-square velocity in any direction. We shall take the time-correlation function $D(t - t')$ as

$$D(t) = \exp(-\tfrac{1}{2}\omega_0^2 t^2), \tag{9}$$

where $\omega_0 \geq 0$, an arbitrary choice, and work with four choices of $E(k)$:

$$\begin{aligned} E_1(k) &= \tfrac{3}{2}v_0^2\, \delta(k - k_0), \\ E_2(k) &= 16(2/\pi)^{1/2} v_0^2 k^4 k_0^{-5} \exp(-2k^2/k_0^2), \\ E_3(k) &= v_0^2\, \delta(k - k_0), \\ E_4(k) &= 4.5 k^3 k_0^{-4} \exp(-\tfrac{3}{2}k^2/k_0^2). \end{aligned} \tag{10}$$

All four choices peak at $k = k_0$. Spectra 1 and 3 describe excitation confined to a thin shell, in three and two dimensions, respectively. Spectra 2 and 4 describe less concentrated excitations, in three and two dimensions, respectively, with excitation intensity per mode proportional to k^2 near $k = 0$.

Three statistical functions of prime interest are the Lagrangian velocity covariance,

$$U_L(t) = \langle v_1(0)v_1(t)\rangle,$$

the effective eddy diffusivity,

$$\kappa(t) = \langle y_1(t)v_1(t)\rangle,$$

and the dispersion,

$$Y(t) = \langle y_1(t)y_1(t)\rangle.$$

Here the subscript 1 denotes the component along any axis. It follows from incompressibility and statistical stationarity of $\mathbf{u}(\mathbf{x}, t)$ that these functions are related by[1,2]

$$\kappa(t) = \int_0^t U_L(s)\,ds, \qquad Y(t) = 2\int_0^t \kappa(s)\,ds. \tag{11}$$

The spectra (10) imply a correlation length $l \sim k_0^{-1}$ for the velocity field. If $\omega_0 \sim v_0/l$, the reciprocal of the eddy circulation time, we expect, following Taylor,[1] that the eddy diffusion will act like a molecular diffusion process, or random walk, with mean free path l and thermal velocity v_0, provided that $\omega_0 t \gg 1$. Then, as $t \to \infty$, we expect that $U_L(t) \to 0$, $\kappa(t)$ approaches a finite limit $\sim v_0 l$, and

$$Y(t) \approx 2\kappa(\infty)t \qquad (v_0 t \gg l). \tag{12}$$

A principal purpose of the present computer experiments is to corroborate these conjectures and to see whether they remain valid when $\omega_0 = 0$, so that the Eulerian velocity field is frozen in time and the fluid particles migrate through the static field according to (1). The static diffusion problem is a simple and severe test for statistical theories.[3]

If the motion does act like a classical diffusion process for long times, we expect the behavior

$$g_k(t) \approx \exp\,[-k^2\kappa(\infty)t] \qquad (kl \ll 1,\ t \gg l/v_0), \tag{13}$$

which implies

$$G_k(0) \approx 1/[k^2\kappa(\infty)] \qquad (kl \ll 1). \tag{14}$$

Equation (13) is the Fourier transform of the Gaussian probability distribution $G(\mathbf{x}, t)$ inferred by Taylor.[1] It implies that at long times the flatness factors of the $\mathbf{y}(t)$ distribution have the Gaussian values

$$\begin{aligned}\langle[y_1(t)]^4\rangle/\langle[y_1(t)]^2\rangle^2 &= 3,\\ \langle|\mathbf{y}(t)|\rangle^4/\langle|\mathbf{y}(t)|^2\rangle^2 &= \tfrac{5}{3},\end{aligned} \qquad \text{(3-D)} \tag{15}$$

$$\begin{aligned}\langle[y_1(t)]^4\rangle/\langle[y_1(t)]^2\rangle^2 &= 3,\\ \langle|\mathbf{y}(t)|^4\rangle/\langle|\mathbf{y}(t)|^2\rangle^2 &= 2.\end{aligned} \qquad \text{(2-D)} \tag{16}$$

On the other hand, for $v_0 t \ll l$, $G(\mathbf{x}, t)$ should differ inappreciably from what it would be if $\mathbf{u}(\mathbf{x}, t)$ were independent of $\mathbf{x}$ and t, provided $\omega_0 \lesssim v_0/l$. Since $\mathbf{u}$ is normal, this again implies Gaussian $G(\mathbf{x}, t)$, but now with[4]

$$g_k(t) \approx \exp\,(-v_0^2k^2t^2/2) \qquad (t \ll l/v_0). \tag{17}$$

Equation (17) implies

$$G_k(0) \approx \frac{(\pi/2)^{1/2}}{(v_0k)} \qquad (kl \gg 1), \tag{18}$$

since, for such high k, $g_k(t)$ is already so small at $t \sim l/v_0$ that (18) holds for all t that contribute appreciably to $G_k(0)$.

If the Eulerian velocity field is frozen, we must recognize the possibility that some of the particles are trapped in closed orbits. This would imply a number of anomalies in the diffusion process, the most striking of which is that $g_k(t)$ tends to finite values as $t \to \infty$ (corresponding to the steady-state distribution of the trapped particles) so that $G_k(0)$ is infinite. Trapping also implies deviation of flatness factors from the normal values (15)–(16). We anticipate trapping in two dimensions, since the stream function of the random velocity field should have maxima and minima with finite probability per unit area, and the streamlines are closed in the neighborhood of these points.

II. COMPUTER SIMULATION

Patterson and Corrsin have described computer simulation of diffusion in one dimension in which a random velocity field was constructed directly on a grid in $\mathbf{x}$ space.[5] In the present studies, the wave-vector components of the velocity field are stored instead, and the field is synthesized in $\mathbf{x}$ space only

[1] G. I. Taylor, Proc. London Math. Soc., Ser. 2, **20**, 196 (1921).
[2] J. L. Lumley, in *Mécanique de la Turbulence* (Centre National de la Recherche Scientifique, Paris, 1962), p. 17.
[3] R. H. Kraichnan, in *Hydrodynamic Instability* (American Mathematical Society, Providence, Rhode Island, 1962), p. 199.
[4] P. H. Roberts, J. Fluid Mech. **11**, 257 (1961).
[5] G. S. Patterson and S. Corrsin, in *Dynamics of Fluids and Plasmas*, S. I. Pai, Ed. (Academic Press Inc., New York, 1966), p. 275.

along the particle trajectories. The velocity field is realized in the form

$$\mathbf{u}(\mathbf{x}, t) = \sum_{n=1}^{N} [\mathbf{v}(\mathbf{k}_n) \cos(\mathbf{k}_n \cdot \mathbf{x} + \omega_n t) + \mathbf{w}(\mathbf{k}_n) \sin(\mathbf{k}_n \cdot \mathbf{x} + \omega_n t)], \quad (19)$$

where

$$\mathbf{v}(\mathbf{k}_n) = \boldsymbol{\zeta}_n \times \mathbf{k}_n, \qquad \mathbf{w}(\mathbf{k}_n) = \boldsymbol{\xi}_n \times \mathbf{k}_n, \quad (20)$$

which insures incompressibility,

$$\mathbf{k}_n \cdot \mathbf{v}(\mathbf{k}_n) = \mathbf{k}_n \cdot \mathbf{w}(\mathbf{k}_n) = 0.$$

The vectors $\boldsymbol{\zeta}_n$ and $\boldsymbol{\xi}_n$ were picked independently from a three- or two-dimensional Gaussian distribution. In accord with (9), the ω_n were picked from a Gaussian distribution with standard deviation ω_0. The vectors $\mathbf{k}_n$ were picked from a statistically isotropic distribution so shaped that the desired $E(k)$ would be realized in the limit $N \to \infty$. For spectra E_1 or E_3, this means that $\mathbf{k}_n$ is isotropically distributed on the surface of a sphere, or circle, of radius k_0. For spectrum E_2, each component of $\mathbf{k}_n$ is picked from a Gaussian distribution of standard deviation $k_0/2$, while, for spectrum E_4, each component of $\mathbf{k}_n$ is picked from a Gaussian distribution of standard deviation $k_0/\sqrt{3}$. By the central limit theorem, $\mathbf{u}(\mathbf{x}, t)$ is normal in the limit $N \to \infty$. All the parameters in (19) are chosen afresh for each realization.

In each realization, (1) is integrated forward by a fourth-order, stable predictor–corrector scheme due to Hamming,[6] after forming starting values by a second-order predictor–corrector method and four iterations of Newton's interpolation formulas for the first three time steps.[6] At each needed point on the trajectory, $\mathbf{u}(\mathbf{x}, t)$ is computed from (19). This process is repeated for R realizations, and the statistical functions are computed as

$$\begin{aligned} U_L(t) &= \frac{1}{3R} \sum_{r=1}^{R} \mathbf{v}_r(0) \cdot \mathbf{v}_r(t), \\ \kappa(t) &= \frac{1}{3R} \sum_{r=1}^{R} \mathbf{y}_r(t) \cdot \mathbf{v}_r(t), \\ Y(t) &= \frac{1}{3R} \sum_{r=1}^{R} |\mathbf{y}_r(t)|^2, \\ g_k(t) &= \frac{1}{R} \sum_{r=1}^{R} \frac{\sin(k\,|\mathbf{y}_r(t)|)}{k\,|\mathbf{y}_r(t)|} \quad \text{(3-D)}, \end{aligned} \quad (21)$$

$$\begin{aligned} U_L(t) &= \frac{1}{2R} \sum_{r=1}^{R} \mathbf{v}_r(0) \cdot \mathbf{v}_r(t), \\ \kappa(t) &= \frac{1}{2R} \sum_{r=1}^{R} \mathbf{y}_r(t) \cdot \mathbf{v}_r(t), \\ Y(t) &= \frac{1}{2R} \sum_{r=1}^{R} |\mathbf{y}_r(t)|^2, \\ g_k(t) &= \frac{1}{R} \sum_{r=1}^{R} J_0(k\,|\mathbf{y}_r(t)|) \quad \text{(2-D)}, \end{aligned} \quad (22)$$

where $\mathbf{v}_r(t)$ and $\mathbf{y}_r(t)$ are the particle velocity and position vectors in the rth realization.

The Gaussian distributions used in the computations are formed by the logarithm, cosine method,[7] starting with pseudorandom uniformly distributed numbers produced by the IBM 360 RANDU routine.[8] In order to minimize effects from spurious correlations, a table of 1000 pseudorandom numbers was set up in advance. The numbers used were then chosen from the table by random addressing, and, once used, each number was replaced by a new pseudorandom number. The results showed no statistically significant deviations from straightforward use of the pseudorandom numbers, however.

Most of the runs to be reported used $N = 100$, $R = 2000$. Runs with $N = 50$ showed no statistically significant deviations.

III. DIRECT-INTERACTION APPROXIMATION

The direct-interaction approximation for diffusion by a random velocity field has been analyzed in detail by Roberts.[4] For velocity correlations of the form (7), (8), the equation for $g_k(t)$ is

$$\frac{dg_k(t)}{dt} = -k \int_0^t D(t-s) \cdot \int_0^\infty p\,dp\,K(p, k) g_p(t-s) g_k(s)\,ds, \qquad g_k(0) = 1, \quad (23)$$

where

$$K(p, k) = \frac{1}{2} \int_{|k-p|}^{k+p} q^{-1} \sin^2(q, k) E(q)\,dq \quad \text{(3-D)}, \quad (24)$$

$$K(p, k) = \frac{2}{\pi} \int_{|k-p|}^{k+p} q^{-1} |\sin(q, k)|\, E(q)\,dq \quad \text{(2-D)}, \quad (25)$$

[6] A. Ralston and H. S. Wilf, *Mathematical Methods for Digital Computers* (John Wiley & Sons, Inc., New York, 1960), p. 100.

[7] M. Abramowitz and I. A. Stegun, Eds., *Handbook of Mathematical Functions* (Dover Publications, Inc., New York, 1965), p. 953.

[8] IBM Scientific Subroutine Package (IBM, Poughkeepsie, New York, 1967).

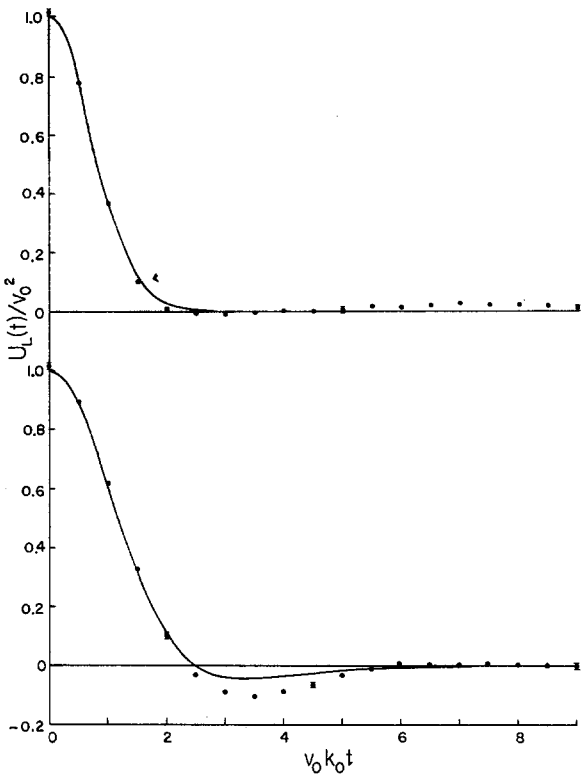

FIG. 1. Lagrangian velocity correlation, three dimensions, spectrum E_1. Points are computer experiment, curves are direct-interaction approximation. Upper data are for $\omega_0 = v_0 k_0$, lower data are for $\omega_0 = 0$.

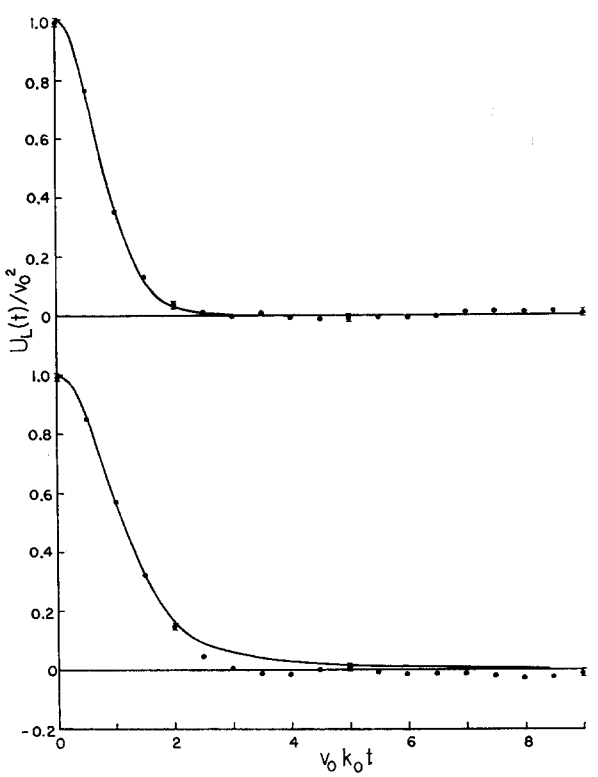

FIG. 2. Lagrangian velocity correlation, three dimensions, spectrum E_2. Points are computer experiment, curves are direct-interaction approximation. Upper data are for $\omega_0 = v_0 k_0$, lower data are for $\omega_0 = 0$.

and $\sin(q, k)$ is the sine of the interior angle opposite p in a triangle with sides k, p, and q. The direct-interaction approximation for $U_L(t)$ is[4]

$$U_L(t) = CD(t) \int_0^\infty E(k) g_k(t)\, dk,$$
$$C = \tfrac{2}{3} \quad \text{(3-D)}, \qquad C = 1 \quad \text{(2-D)}, \tag{26}$$

and $\kappa(t)$, $Y(t)$ are given by (11). The approximation (26) for $U_L(t)$ in terms of the Eulerian velocity correlation was suggested independently by Saffman.[9] The direct-interaction gives the long-time behavior (13), (14), if $\kappa(\infty)$ is finite.[4] But instead of (17) and (18), it gives

$$g_k(t) \approx J_1(2v_0 kt)/(v_0 kt) \qquad (t \ll l/v_0), \tag{27}$$

$$G_k(0) \approx 1/(v_0 k) \qquad (kl \gg 1). \tag{28}$$

Equation (27) implies that $G(\mathbf{x}, t)$ at short times has a peculiar cusped form,[4] instead of the correct Gaussian form.

If $\omega_0 = 0$, so that $D(t) = 1$, the Laplace transform of (23) is

$$G_k(u) = \left(u + k \int_0^\infty p\, dp\, K(p, k) G_p(u)\right)^{-1}, \tag{29}$$

in which the different frequencies are uncoupled.

Equation (23) was integrated in time by the same scheme used for (1). The time integrals on the right-hand side were evaluated by Simpson's rule, using the "$\frac{3}{8}$" rule for the last three panels when the number of panels was odd. The wavenumber integrations in (23)–(25) were done by the trapezoidal rule. Because of the sine factors, the integrands vanish at the end points, with the result that the trapezoidal rule integration has accuracy equivalent to Simpson's rule. In addition, (29) was solved by an iterative procedure to yield values for $G_k(0)$. Equations (23) and (29) were integrated for k up to a cutoff value $k_{\max}$. The p integrals were continued for $p > k_{\max}$ up to values where $K(p, k)$ became negligible due to the high-wavenumber falloff of $E(q)$. The needed values of $g_k(t)$ and $G_k(0)$ for $k > k_{\max}$ were approximated by replacing $g_p(t - s)$ and $G_p(0)$ in the integrands by $g_k(t - s)$ and $G_k(0)$ so that uncoupled equations resulted which could be solved for each needed $k > k_{\max}$. [For $\omega_0 = 0$,

[9] P. G. Saffman, Appl. Sci. Res. A11, 245 (1962).

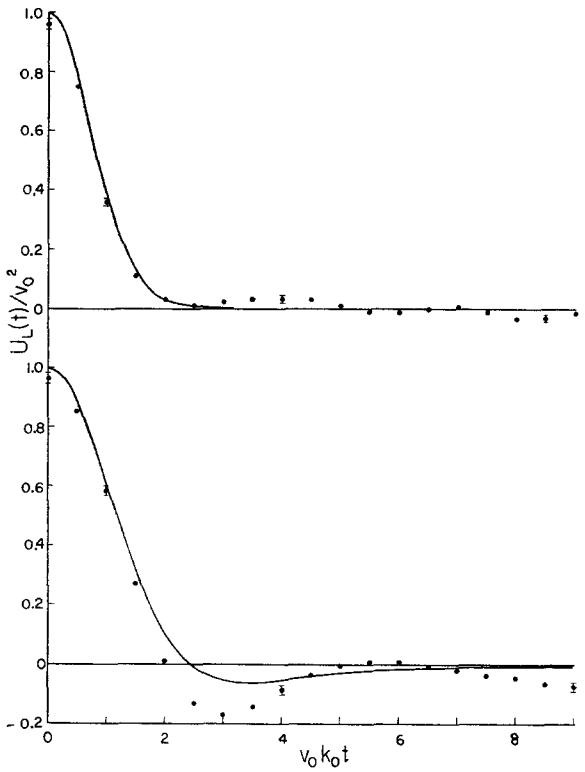

FIG. 3. Lagrangian velocity correlation, two dimensions, spectrum E_3. Points are computer experiment, curves are direct-interaction approximation. Upper data are for $\omega_0 = v_0k_0$, lower data are for $\omega_0 = 0$.

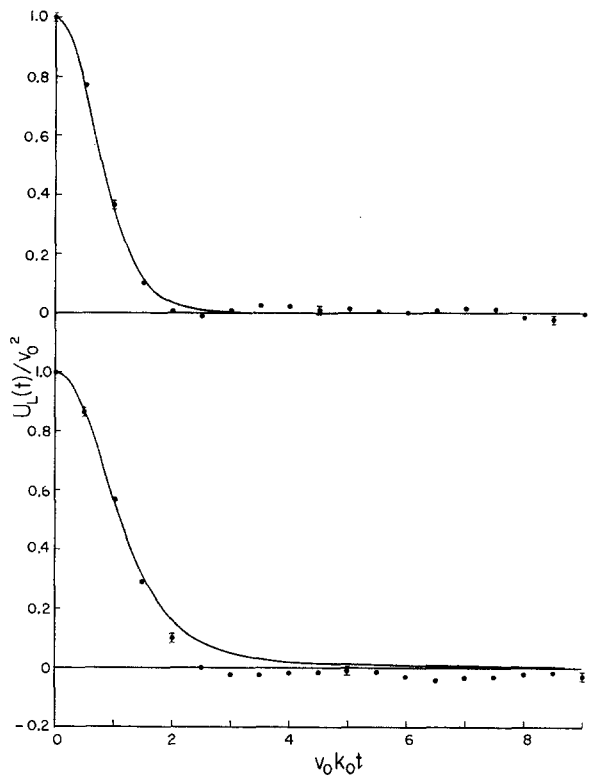

FIG. 4. Lagrangian velocity correlation, two dimensions, spectrum E_4. Points are computer experiment, curves are direct-interaction approximation. Upper data are for $\omega_0 = v_0k_0$, lower data are for $\omega_0 = 0$.

this is equivalent to using the high k limit forms (27) and (28).] The over-all numerical accuracy was tested by varying grid sizes and cutoffs. Errors in the results presented are too small to show up on the plots.

IV. RESULTS

Figures 1–4 show values of $U_L(t)$ obtained from the computer experiments and the direct-interaction equations for the four spectra (10) and for two values of ω_0 in (9): $\omega_0 = 0$ and $\omega_0 = v_0k_0$. Figures 5–8 show values of $Y(t)$ and $\kappa(t)$ for some of these cases. In these, and following plots, the bars attached to the computer-experiment points show probable errors, which were computed from variances of the functions in standard fashion. Except as noted under Fig. 8, all of the simulation runs used $N = 100$, $R = 2000$. Truncation and discretizing errors appear to be small compared with the statistical fluctuations in all the plots. Figure 9 shows the flatness factor of the distribution of $r = |\mathbf{y}|$ for four of the simulation runs. Direct-interaction calculations of this quantity were not made. Figures 10–16 show comparisons of $g_k(t)$ and $G_k(0)$ from simulation runs, direct-interaction solutions, and the asymptotic formulas of Sec. I.

With the exception of the frozen-Eulerian-field runs ($\omega_0 = 0$) in two dimensions, all of the results appear to be consistent with Taylor's picture of a classical diffusion process at long times ($v_0k_0t \gg 1$). That is, $\kappa(\infty)$ takes a value $\sim v_0k_0^{-1}$ and (12) appears to be valid, while the flatness factor (Fig. 9) takes the Gaussian values (15), (16) for long times. In all the cases where there is classical behavior, the direct-interaction results appear to be good approximations.

The simulation run in two dimensions with spectrum E_3 and $\omega_0 = 0$ shows anomalies which appear to be clearly associated with trapping. Similar results (not plotted) were found for spectrum E_4 at $\omega_0 = 0$. The clearest evidences of trapping are the non-Gaussian behavior of the flatness factor (Fig. 9) and the leveling off of $g_k(t)$ at finite values for long t (Fig. 15). It is not clear from Fig. 7 whether the particles which are not trapped yield a classical diffusion satisfying (12). The direct-interaction results for this case completely fail to describe the trapping and give large errors in $Y(t)$ as well as in

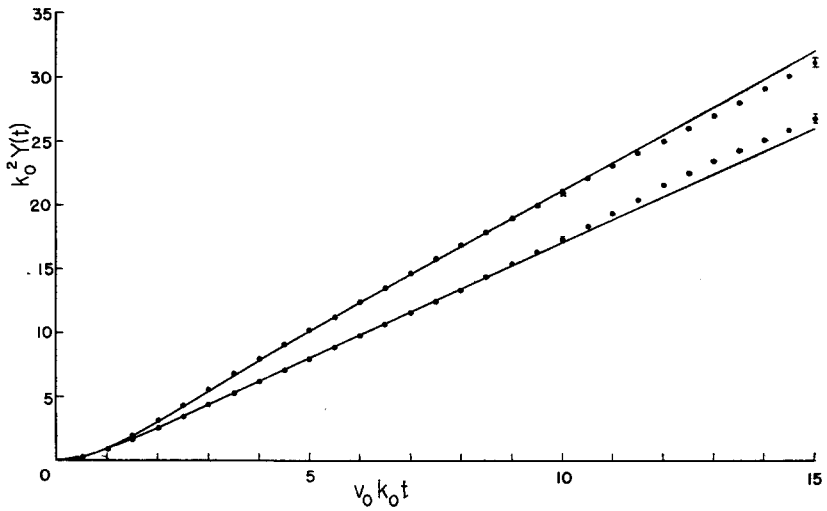

FIG. 5. Dispersion vs time, three dimensions, spectrum E_1. Upper curve and points, direct-interaction approximation and computer experiment for $\omega_0 = 0$. Lower curve and points for $\omega_0 = v_0 k_0$.

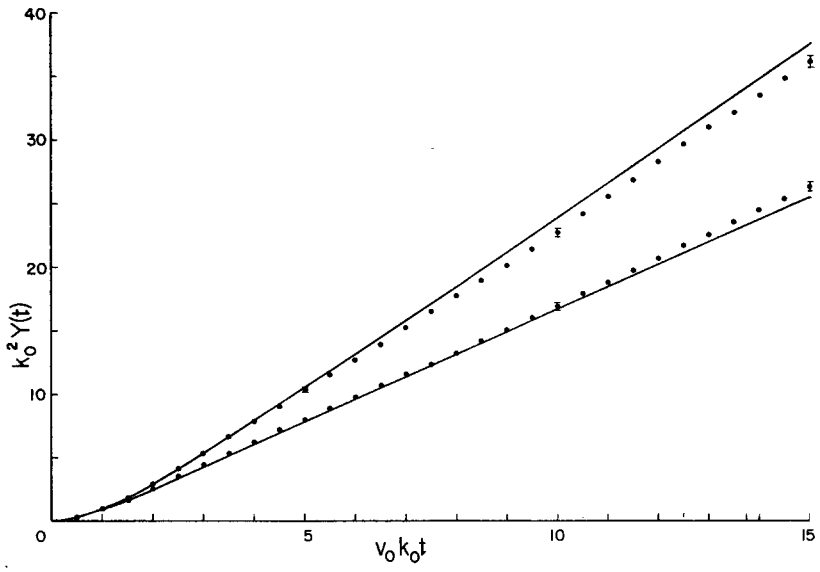

FIG. 6. Dispersion vs time, three dimensions, spectrum E_2. Upper curve and points, direct-interaction approximation and computer experiment for $\omega_0 = 0$. Lower curve and points for $\omega_0 = v_0 k_0$.

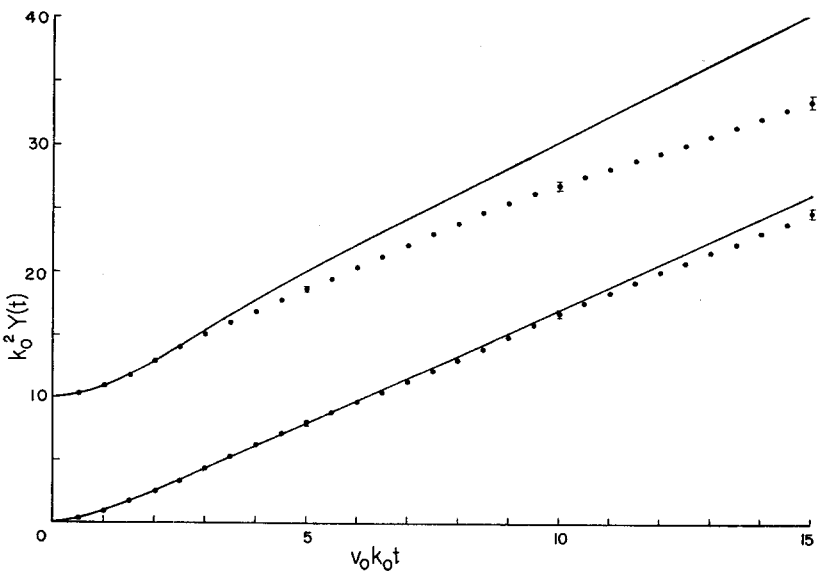

FIG. 7. Dispersion vs time, two dimensions, spectrum E_3. Upper curve and points, direct-interaction approximation and computer experiment for $\omega_0 = 0$. Lower curve and points for $\omega_0 = v_0 k_0$. Vertical scale for upper data is displaced by 10 units.

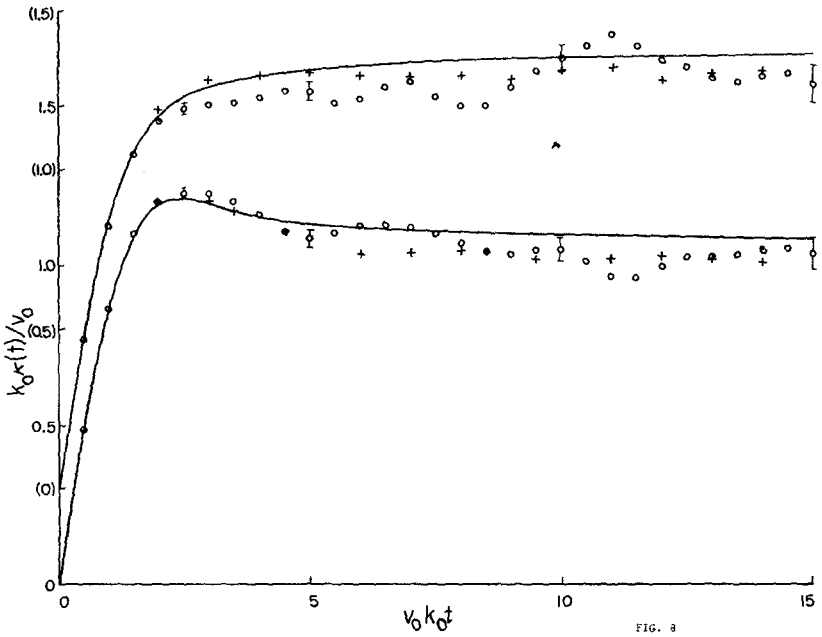

FIG. 8. Eddy diffusivity vs time for frozen Eulerian field, three dimensions. Upper data and scale ( ) are for spectrum E_2, lower data for spectrum E_1. Curves are direct-interaction approximation, circles are numerical experiments with $N = 100$, $R = 2000$. For lower plus signs, $N = 50$, $R = 23\,750$. For upper plus signs, $N = 50$, $R = 21\,000$.

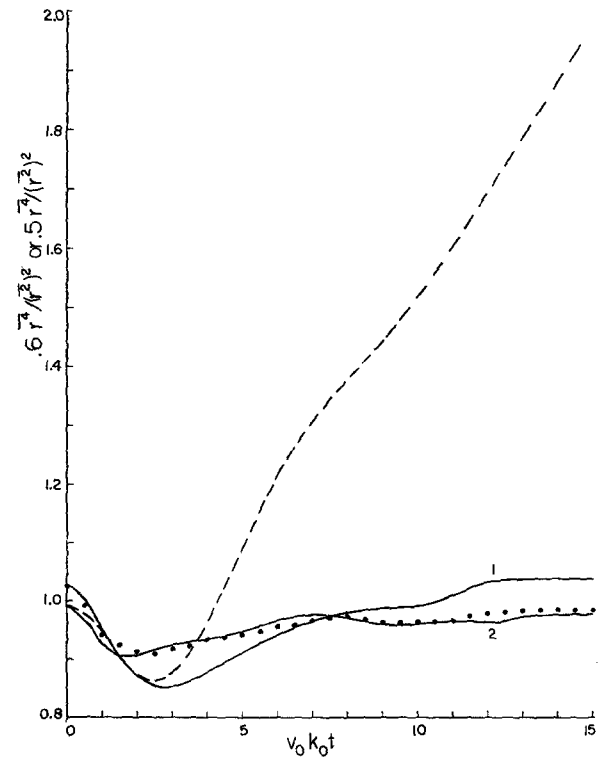

FIG. 9. Flatness factor of $r = |y|$ vs time for numerical experiments. Curve 1, three dimensions, spectrum E_1, $\omega_0 = 0$. Points, three dimensions, spectrum E_1, $\omega_0 = v_0 k_0$. Dashed curve, two dimensions, spectrum E_2, $\omega_0 = 0$. Curve 2, two dimensions, spectrum E_2, $\omega_0 = v_0 k_0$. Normalization 0.6 is for three dimensions, 0.5 is for two dimensions [Eqs. (15), (16)].

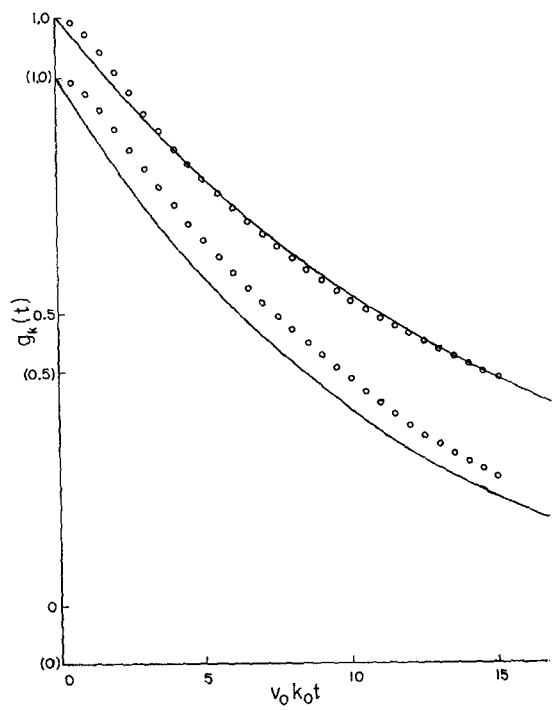

FIG. 10. Test of Eq. (13), three dimensions, $\omega_0 = 0$. Upper points and curve, spectrum E_1. Lower points and curve, spectrum E_2. Points give $g_k(t)$ from computer experiments with $k = 0.25 k_0$. Curves give Eq. (13), with $\kappa(\infty)$ taken from the experiments. [Scale ( ) for E_2.]

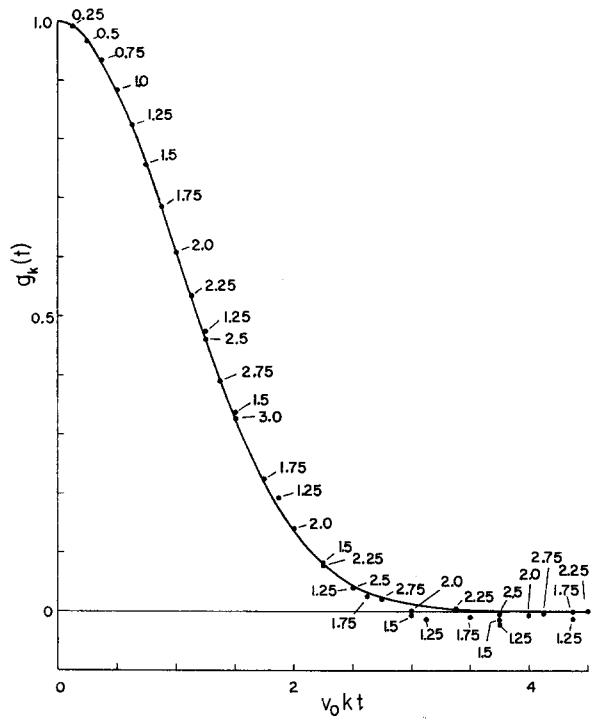

FIG. 11. Test of Eq. (17) against computer experiment, three dimensions, spectrum E_1, $\omega_0 = 0$. The curve is Eq. (17). The points are labeled by the values of k/k_0.

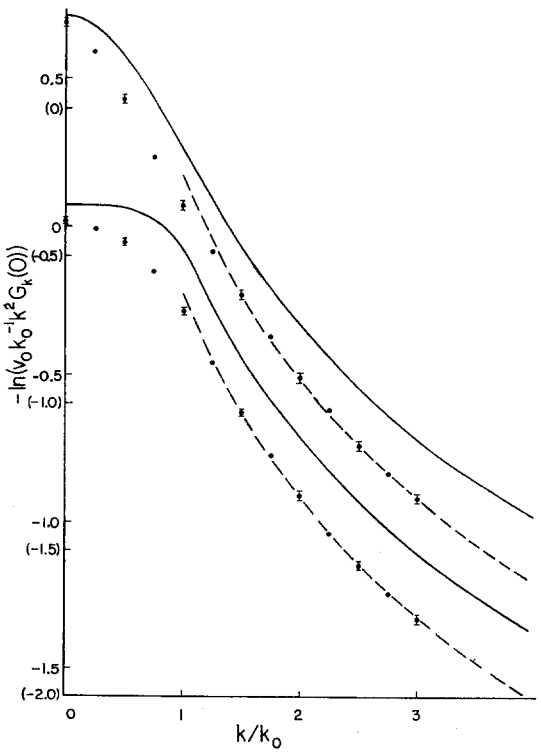

FIG. 12. $G_k(0)$ for three dimensions, $\omega_0 = 0$. Upper points and curves, spectrum E_2. Lower points and curves, spectrum E_1. Points are computer experiment, solid curves are direct-interaction approximation, dashed curves are Eq. (18). [Scale ( ) for E_2.]

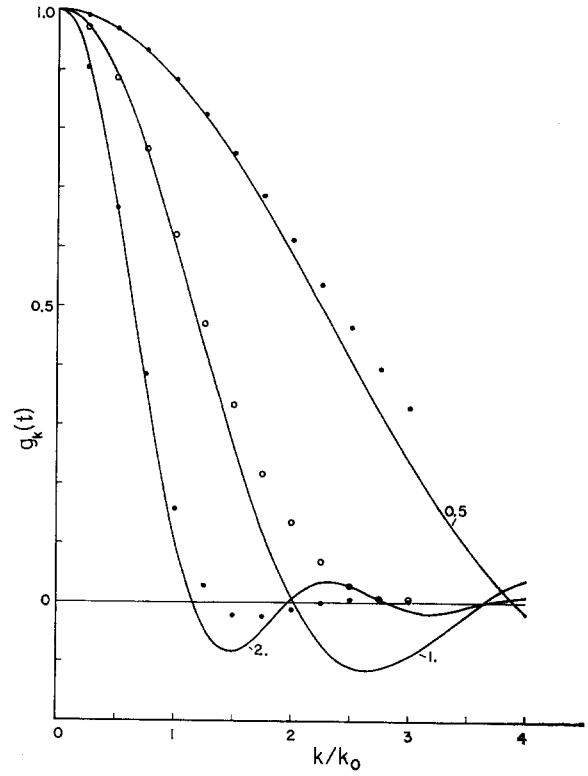

FIG. 13. Values of $g_k(t)$, three dimensions, $\omega_0 = 0$, spectrum E_1. Curves are direct-interaction values, labeled by value of v_0k_0t. Points and circles are corresponding computer-experiment values.

$g_k(t)$. The simulation run for spectrum E_4 at $\omega_0 = v_0k_0$ shows no evidence of trapping, and the direct-interaction results seem as good as for the three-dimensional cases. No evidence of trapping appears in three dimensions even for $\omega_0 = 0$.

An interesting feature in the frozen-field runs for the δ-function spectra (E_1 and E_3) is the pronounced negative region in $U_L(t)$, a characteristic which is reproduced, although underestimated, by the direct-interaction approximation. This phenomenon is associated with the strong negative region in the spatial correlation function of the Eulerian velocity field, which is implied by (7), (8), with a δ-function spectrum.

Figure 10 tests (13) against the three-dimensional, frozen-field simulations. Here, $\kappa(\infty)$ is estimated as the average value of $\kappa(t)$ over the interval $10 \leq v_0k_0t \leq 15$. Similar results were obtained for all other runs, with the exception of the two-dimensional frozen-field cases. Figure 11 is a test of (17). This asymptotic relation appears to be a good approximation even when the validating inequality is substantially violated. Figure 12 shows the modal relaxation time $G_k(0)$ for the three-dimensional,

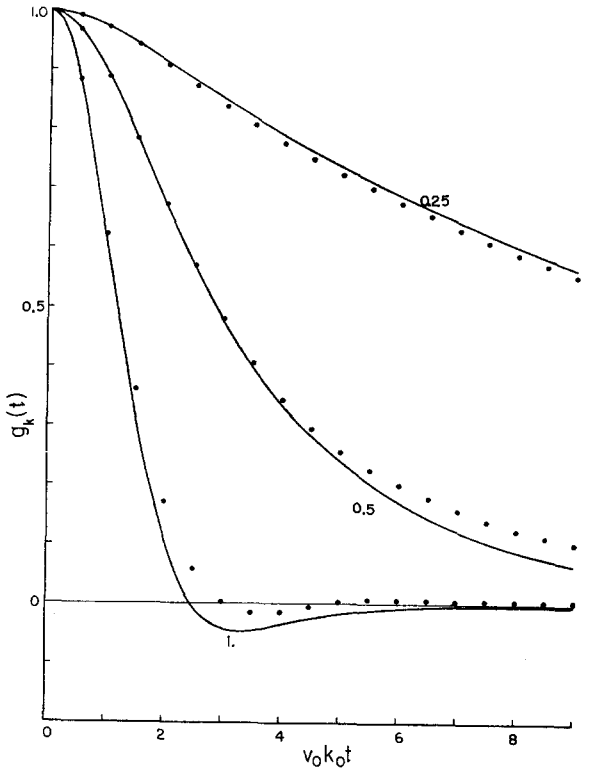

FIG. 14. Values of $g_k(t)$ vs time, three dimensions, $\omega_0 = 0$, spectrum E_1. Curves are direct-interaction values, labeled by values of k/k_0. Points are corresponding computer-simulation values.

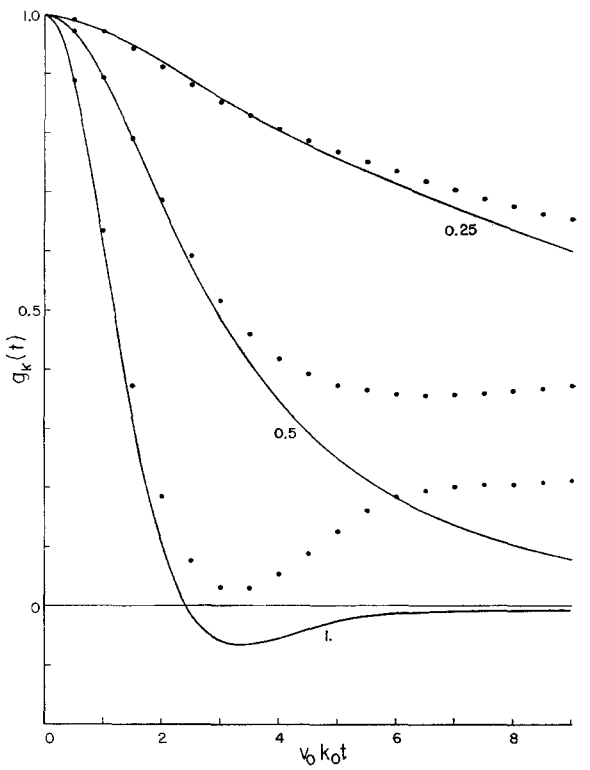

FIG. 15. Values of $g_k(t)$ vs time, two dimensions, $\omega_0 = 0$, spectrum E_3. Curves are direct-interaction values, labeled by values of k/k_0. Points are corresponding computer-simulation values.

frozen-field runs, together with the asymptotic curve (18) and the direct-interaction results obtained from solution of (29). The simulation runs were continued to $v_0 k_0 t = 15$, by which time the quantities

$$\int_0^t g_k(s)\, ds$$

appeared to have reached steady values, to within the statistical fluctuation, for all $k/k_0 \geq 0.75$. The points in Fig. 12 for $k/k_0 = 0.5$ and $k/k_0 = 0.25$ were obtained by fitting $g_k(t)$ to an exponential decay over the interval $10 \leq v_0 k_0 t \leq 15$ and then extrapolating to $t = \infty$. The points at $k = 0$ are the values of $\kappa(\infty)$, estimated as the average of $\kappa(t)$ over the same interval. The largest errors in the direct-interaction values for $G_k(0)$ appear to be at high k, where the computed results follow (28) closely.

Figures 13 and 14 compare simulation and direct-interaction results for $g_k(t)$, $k \leq k_0$, with spectrum E_1 (three dimensions) and frozen Eulerian field. For k/k_0 substantially greater than one (not plotted), the values are inessentially different from the asymptotic forms (17) and (27). Figures 15 and 16 repeat Figure 14, but in two dimensions with δ-function spectrum and with frozen and time-varying Eulerian fields, respectively. The differences between Figs. 15 and 16 show that the fidelity of the direct-interaction approximation depends strongly on absence of trapping.

If the correlation time of the Eulerian velocity field is very short compared with the eddy circulation time ($\omega_0 \gg v_0 k_0$), the Eulerian and Lagrangian velocity covariances are almost the same, the diffusion is almost Markovian, and the direct-interaction approximation is asymptotically exact.[10] The frozen and slowly varying fields we have examined, therefore, are the most critical tests of the direct-interaction equations. This leaves open the question of how performance holds up for velocity spectra $E(k)$ which are less concentrated about k_0 than the cases treated here. The higher statistics of the velocity field are critically important in this connection. Multivariate normal statistics preclude representation of the convection of small scales by large scales

[10] R. H. Kraichnan, Phys. Fluids 11, 945 (1968).

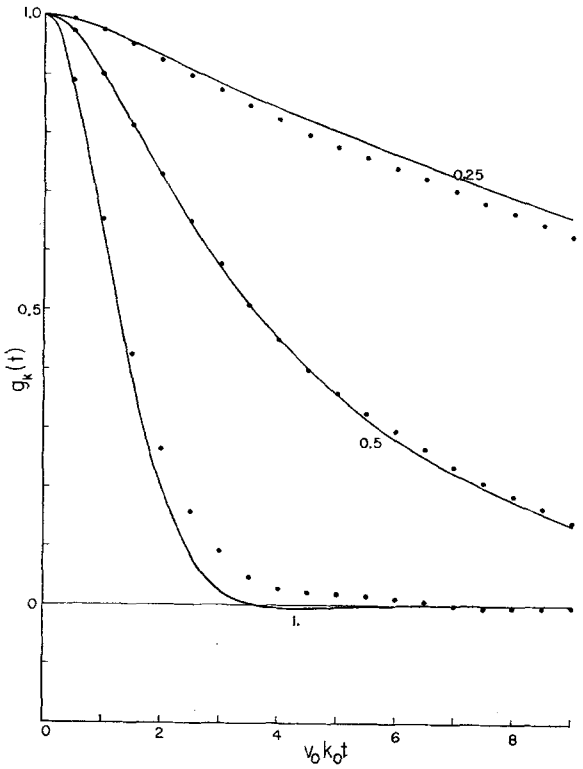

FIG. 16. Values of $g_k(t)$ vs time, two dimensions, $\omega_0 = v_0 k_0$, spectrum E_3. Curves are direct-interaction values, labeled by values of k/k_0. Points are corresponding computer-simulation values.

that is characteristic of actual turbulence. The different scales are independent, with the result that the strongly excited large scales of a typical spectrum whip the fluid particles rapidly through the small scales and reduce the effective diffusivity due to the latter below what it would be in actual turbulence. In the direct-interaction approximation, the effective dynamical time of small scales is the sweep-past time associated with motion at large-scale velocity, so that this interference effect of different scales, expected with multivariate normal statistics, should be well represented. We therefore expect no deterioration of accuracy with more diffuse spectra, an anticipation supported by the results obtained here, which show greater accuracy for spectrum E_2 than for E_1. On the other hand, the input to the direct-interaction equation is exclusively the Eulerian velocity covariance, which carries insufficient information to describe the convection effects of actual turbulence; there is no way to get the associated nonnormal statistics into the approximation, if we should desire to work with real turbulence.[11] The quantitative errors in $U_L(t)$, $\kappa(t)$, and $Y(t)$ associated with misrepresentation of of convection effects may be small, however, even at high Reynolds numbers, because these quantities are dominated by contributions from the large scales.

ACKNOWLEDGMENTS

I am very grateful to Dr. J. R. Herring for collaboration in the numerical studies and to Professor S. Corrsin for helpful discussions.

This work was supported by the Office of Naval Research, Fluid Dynamics Branch, under Contract N00014-67-C-0284.

[11] R. H. Kraichnan, Phys. Fluids **7**, 1723 (1964).